


Cite this: *Mater. Horiz.*, 2024, 11, 2180Received 19th October 2023,  
Accepted 8th January 2024

DOI: 10.1039/d3mh01731a

rsc.li/materials-horizons

# Bio-inspired facile strategy for programmable osmosis-driven shape-morphing elastomer composite structures†

Yuanhang Yang,<sup>a</sup> Yueying Wang,<sup>a</sup> Marcus Lin,<sup>a</sup> Mingchao Liu<sup>\*ab</sup> and Changjin Huang <sup>\*a</sup>

Achieving programmable and reversible deformations of soft materials is a long-standing goal for various applications in soft robotics, flexible electronics and many other fields. Swelling-induced shape morphing has been intensively studied as one of the potential mechanisms. However, achieving an extremely large swelling ratio (>1000% in volume) remains challenging with existing swellable soft materials (e.g., hydrogels and water-swellable rubbers). Inspired by the shape change enabled by the osmosis-driven swelling in living organisms, herein, we report a polymer composite system composed of fine sodium chloride (NaCl) particles embedded in Ecoflex<sup>00-10</sup> polymer. This Ecoflex<sup>00-10</sup>/NaCl polymer composite can achieve controllable volumetric swelling up to 3000% while maintaining a relatively high elastic stiffness. We demonstrate that this swellable polymer composite can serve as an active component to drive the shape morphing of various structures. By controlling the geometric design and the fraction of the NaCl particle, morphing structures capable of deforming sequentially are created. Finally, by encapsulating 3D printed polymer composite patterns using water-permeable PDMS membrane, a programmable braille with visual and tactile regulation is demonstrated for the purpose of information encryption. Our study provides a facile approach to generate customizable shape-morphing structures, aiming to broaden the range of techniques and applications for morphing devices.

## 1. Introduction

Within biological systems, numerous organisms possess the ability to modify their shapes or configurations in response to

### New concepts

In this manuscript, the concept of bioinspired osmosis-driven swelling in polymer composites has been demonstrated to achieve a record-breaking improvement in the swelling capability of soft materials. The swelling capacity of soft materials largely determines the morphing capability of solvent-responsive systems. Existing solvent-responsive materials, especially hydrogels and elastomers, are limited to a volumetric swelling ratio of <1000% and often have a trade-off between mechanical stiffness and swelling capacity. Inspired by the osmosis-driven expansion of biological tissues, we demonstrate a strategy to endow Ecoflex, a water-unswellable polymer, with remarkable swelling capability in water by incorporating fine sodium chloride particles. This approach allows for controllable volumetric swelling ratios of up to 3000%, while retaining relatively high elastic stiffness. The swelling kinetics can be programmed through the control of the volume ratio of the sodium chloride particles. Leveraging these swellable polymers as active components, we design diverse shape-morphing structures with varying geometries. Notably, we achieve sequentially deforming shape-morphing structures by modulating swelling characteristics and the geometric design of the polymer composite and design a programmable braille system with visual and tactile regulation for information encryption by encapsulating 3D-printed polymer composite patterns with a water-permeable PDMS membrane.

environmental stimuli, serving as a means for survival, adaptation, and evolution.<sup>1,2</sup> Notable examples include *Bauhinia* seedpods, which undergo twisting motions in response to humidity changes to facilitate seed release,<sup>3</sup> *Mimosa pudica* leaflets that rapidly contract upon touch,<sup>4</sup> and mollusks that adjust their postures through muscular contractions and extensions.<sup>5</sup> While these shape transformations are triggered by diverse stimuli, they share a common mechanism: the regulation of individual cell sizes at the microscopic level is facilitated by the influx and/or efflux of water. Drawing inspiration from these natural paradigms, extensive research has been focused on developing biomimetic solvent-responsive shape-morphing systems. These systems exhibit the ability to alter their shape, size or overall morphology when exposed to specific solvents. Their applications encompass a range of

<sup>a</sup> School of Mechanical and Aerospace Engineering, Nanyang Technological University, Singapore 639798, Singapore. E-mail: mingchao.liu@ntu.edu.sg, cjhuang@ntu.edu.sg

<sup>b</sup> Department of Mechanical Engineering, University of Birmingham, Birmingham B15 2TT, UK

† Electronic supplementary information (ESI) available. See DOI: <https://doi.org/10.1039/d3mh01731a>



fields, such as drug delivery systems that enable controlled release of drugs in response to specific tissue micro-environments,<sup>6</sup> flexible electronics and soft robotics capable of shape change or actuation based on environmental cues,<sup>7–9</sup> biomedical implants that exhibit shape or property adaptations in response to specific solvents encountered within the body,<sup>10</sup> and tissue engineering where scaffolds undergo shape transformations to replicate the natural structures of tissues and organs.<sup>11</sup>

The swelling capability of smart materials plays a pivotal role in the design of solvent-responsive shape-morphing systems.<sup>12</sup> Over time, various solvent-responsive materials have been developed, mainly including hydrogels and elastomers.<sup>13,14</sup> The swelling behavior of hydrogels arises from the hydrophilic nature of their polymeric network, which facilitates the absorption and retention of substantial amounts of water. However, their practical application prospects are hindered by limitations such as low mechanical strength, poor printability, and other drawbacks.<sup>15</sup> In contrast, elastomers generally exhibit better mechanical strength and printability compared to hydrogels, yet their swelling capability in aqueous solutions is usually inconspicuous. Commercial elastomers primarily exhibit significant swelling in organic solvents,<sup>16,17</sup> such as tetrahydrofuran and chloromethane, which are often volatile, toxic and have adverse effects on human health and the environment.<sup>18,19</sup> As an alternative approach, elastomers can be endowed with water-swelling capability by introducing hydrophilic components, such as ethylene-vinyl acetate-methacrylate terpolymer (PEVAcMA), precipitated silica, reactive clay, styrene-acrylonitrile copolymer (SAN), *etc.*<sup>20,21</sup> These reported systems, however, generally exhibit limited swelling capacity, typically below 1000% in volume.<sup>20,21</sup> Inspired by the osmosis-driven swelling phenomena observed in biological organisms, we have devised a unique polymer blend system by incorporating sugar or salt powders into elastomers.<sup>22,23</sup> Notably, the Ecoflex<sup>00-10</sup>/NaCl polymer composite exhibits a substantial swelling in water (~3000% in volume) while maintaining excellent mechanical properties, therefore surpassing the performance of hydrogels and previously reported water-swellaable rubbers (Fig. 1).

Apart from selecting solvent-responsive materials, ingenious structural designs also play a crucial role in achieving desired three-dimensional (3D) shape-morphing behavior.<sup>12</sup> Generally, solvent-responsive 3D shape morphing relies on the differential swelling in multi-component systems. One of the fundamental structures is a bilayer structure composed of two sections with distinct materials. The disparate responses of these layers to solvent induce curvature formation due to their strain mismatch.<sup>33,34</sup> Furthermore, more intricate 3D shapes can be attained by incorporating additional components or arranging different components into elaborate patterns.<sup>35,36</sup> In this study, we systematically investigate the swelling behavior of Ecoflex<sup>00-10</sup>/NaCl polymer composite. By leveraging the strain mismatch between the polymer composite and PDMS in response to water, we engineer various shape-morphing structures capable of achieving programmed and reversible 3D shape changes. By semi-embedding swellable polymer composite into PDMS as hinges to mimic finger joints, we successfully resemble the sequential bending of human fingers. Finally, by taking advantage of the capabilities of 3D printing technology, we demonstrate the potential application of our polymer composite-based shape-morphing system for information encryption. Our study paves the way for the development of intelligent devices.

## 2. Results and discussion

### 2.1. Swelling of the bio-inspired soft polymer composite

Many organisms in nature possess the ability to alter their shapes or configurations in response to osmotic pressure. Fig. 2(a) illustrates the response of a black fungus to osmotic pressure. In its dry state, it appears wizened and small, exhibiting rolled sections. However, upon immersion in water for a certain duration, it undergoes substantial volume expansion. The rolled sections unroll due to the differential swelling experienced by the top and bottom parts of the tissue (Fig. 2(a)). Notably, this process is reversible through dehydration. The generality of this shape change through swelling-dehydration mechanism can be observed in many other

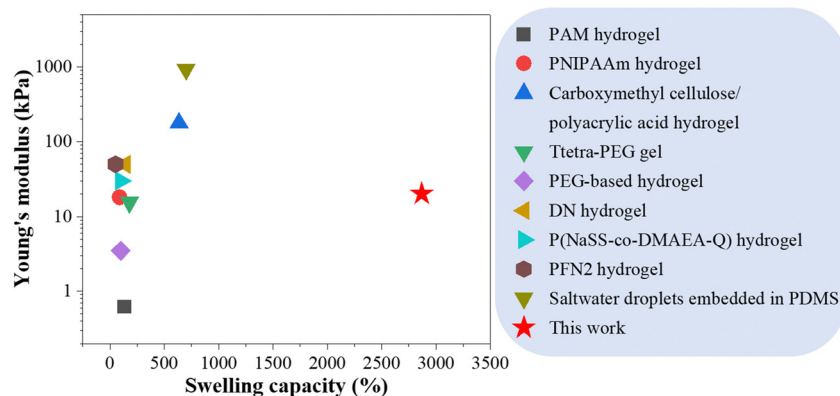
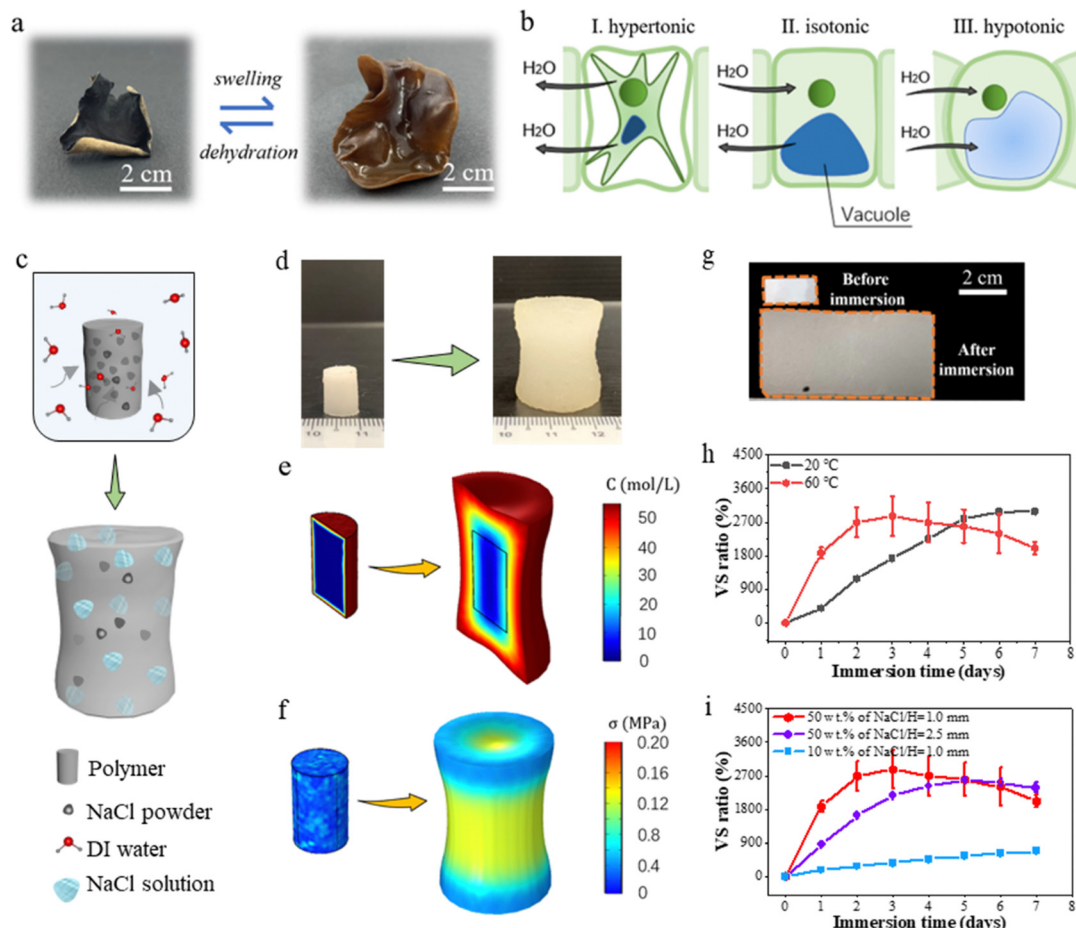


Fig. 1 Comparison of the volumetric swelling capacity and the corresponding Young's modulus between Ecoflex<sup>00-10</sup>/NaCl polymer composite and other swellaable soft materials reported in literatures.<sup>24–32</sup>





**Fig. 2** Swelling of bio-inspired soft polymer composite. (a) Shape change of a black fungus as a result of swelling or dehydration. (b) Schematic illustration of the shape change of a plant cell under different osmotic conditions. (c) Schematic illustration of the swelling process of the Ecoflex<sup>00-10</sup>/NaCl polymer composite. (d) Images of a cylindrical polymer composite sample before and after soaking in water for 3 days. (e) and (f) COMSOL simulation of the cylindrical sample showing the change in ion concentration and von Mises stress distribution as a result of swelling. (g) Representative images of the Ecoflex<sup>00-10</sup>/NaCl polymer composite sheet before and after 3 days of swelling. (h) Volume swelling ratio of the polymer composite sheet with 50 wt% NaCl as a function of immersion duration in water under different temperatures. (i) Effects of sample thickness and NaCl concentration on the swelling kinetics of the polymer composite sheet in water under 60 °C.

biological tissues (see Fig. S1, ESI†). In biology, it is essential for cells to be able to regulate its water content to prevent excessive swelling or shrinkage which is detrimental to the cell structures. The regulation of water content in cell is manifested in Fig. 2(b). When its intracellular and extracellular environments have an equal osmotic pressure (*i.e.*, isotonic condition), the inward and outward water fluxes are always in a perfect balance, and the size of a cell remains unchanged. On the other hand, it shrinks (swells) when the extracellular environment is changed to be hypertonic (hypotonic) as the outward flux exceeds (falls behind) the inward flux.<sup>37</sup>

Inspired by osmotic pressure-induced swelling of biological tissues, we mix NaCl powders with Ecoflex<sup>00-10</sup> to form an elastomer-salt polymer composite in which each NaCl powder functions as an individual biological cell while the Ecoflex<sup>00-10</sup> polymer functions as plasma membrane. The Ecoflex<sup>00-10</sup> polymer is selected as the elastomeric matrix considering its outstanding stretchability and water permeability, and the NaCl

powders are adopted in view of their ultra-high solubility in water. As illustrated in Fig. 2(c), when the composite is immersed in water, water molecules diffuse through the polymer matrix and dissolve the NaCl powders, leading to a high concentration gradient of Na<sup>+</sup> and Cl<sup>-</sup> ions at the interface. The corresponding high osmotic pressure gradient then pumps more water into the polymer composite, causing a large volume expansion of the polymer composite.

To demonstrate the expected swelling phenomenon, we construct a cylindrical sample made of the Ecoflex<sup>00-10</sup>/NaCl polymer composite, exhibited in Fig. 2(d). After immersing in water for 3 days, the sample swells more than 800% in volume. Noted the concentration gradient between the center and the edge decreases as the swelling ratio increases, as shown in Fig. 2(e). More interestingly, as the swelling progresses, the cylinder evolves into a dumbbell shape. Such a shape change is caused by the residual stress resulted from the differential swelling between the center and the edge region. As water



molecules diffuse from the edge towards center, it leads to a gradient in the swelling level from the edge to the center. The stress distribution becomes uneven where larger stress exists at the center while smaller stress is distributed at the edge, as shown in Fig. 2(f). Similar swelling responses are also observed in samples prepared using several other water-unswellable polymers, including Ecoflex<sup>00-30</sup>, Ecoflex<sup>00-50</sup> and PDMS, confirming the general applicability of the osmosis-driven swelling of polymer/NaCl composites (Fig. S2, ESI†).

To evaluate possible contribution by capillary adsorption resulting from the interfacial gap between particles and the polymer matrix, in addition to NaCl particles, we also mixed the Ecoflex<sup>00-10</sup> polymer with chitosan and graphite particles at a concentration of 10 wt% (Fig. S3(a), ESI†). The cross-sectional morphologies of the three polymer composites are exhibited in Fig. S3(b) (ESI†). Unlike NaCl, both chitosan and graphite are nearly insoluble in water. As shown in Fig. S3(c and d) (ESI†), the Ecoflex<sup>00-10</sup>/chitosan and Ecoflex<sup>00-10</sup>/graphite polymer composites exhibit a water absorption and volume swelling ratio of less than 10%, whereas the Ecoflex<sup>00-10</sup>/NaCl composite displays a significantly higher water absorption of more than 500% and volume swelling ratio of 700% under the same condition. The results confirm that osmotic pressure plays a dominant role in driving the swelling of the Ecoflex<sup>00-10</sup>/NaCl polymer composite.

To understand and harness the swelling behavior of the Ecoflex<sup>00-10</sup>/NaCl polymer composite, we conduct systematic investigation using a thin polymer composite sheet with dimensions of 20 × 10 × 1 mm, as shown in Fig. 2(g). Intuitively, the swelling rate is expected to positively correlate with the diffusion coefficient of water molecules since the swelling process requires water molecules to diffuse through the polymer matrix. The influence of temperature on the diffusion of water can be rationalized using the Arrhenius equation, *i.e.*,

$D \sim e^{-\frac{E_a}{RT}}$ , where  $D$ ,  $E_a$ ,  $R$ , and  $T$  denote the diffusion coefficient, activation energy of diffusion, gas constant and temperature, respectively.<sup>38</sup> Consequently, a higher temperature  $T$  leads to a larger  $D$  and therefore a higher swelling rate. Indeed, when immersed the sample in DI water under 60 °C, a significantly higher swelling rate is observed than that under 20 °C. Albeit in both conditions a maximum volume swelling ratio of approximately 2900% is ultimately obtained, the sample reaches this ratio in 3 days under 60 °C while in 6 days under 20 °C (Fig. 2(h)).

The swelling process is also heavily influenced by the mass fraction of the NaCl powders. As shown in Fig. 2(i), the sample with 10 wt% of NaCl powders exhibits a much smaller volume swelling ratio and a slower swelling rate compared to the sample with 50 wt% of NaCl powders over a 7-day period. The swelling responses of the Ecoflex<sup>00-10</sup>/NaCl polymer composites with a broader NaCl concentration range over a much longer immersion time (up to 17 days) indicate that there is a trade-off between the swelling rate and the long-term stability of the swelled structure. More specifically, a higher NaCl content corresponds to a larger swelling rate but also a more fast and significant volume reduction due to the release of Na<sup>+</sup>

and Cl<sup>−</sup> ions (Fig. S4(a and b), ESI†). The thickness of the sample has a non-negligible impact on the swelling kinetics. Since swelling always starts from the outmost layer of the sample and then gradually propagates towards inside, the inner part that is less swelled or has not been swelled constrains the expansion of the outer layer. Consequently, a thinner sample suffers from less resistance from the inner part and exhibits a faster swelling process. Consistently in our experiments, the 1 mm-thick sample exhibits a relatively higher swelling rate than the one with a thickness of 2.5 mm (Fig. 2(i)). In addition, the swelling responses of the polymer composites are significantly influenced by the NaCl concentration in the external solution. As shown in Fig. S4(c and d) (ESI†), the swelling ratio of the polymer composites reduces with the increase in the NaCl concentration in the external solution, and negligible swelling is observed in the saturated NaCl solution, which further confirms that osmotic pressure is the primary driving force for the swelling of the polymer composite. The amount of water used to submerge the samples can also regulate the swelling responses of the polymer composite. Fig. S4(e and f) (ESI†) shows the water absorption and volume swelling ratio of the polymer composite during soaking in 10 mL, 300 mL, and 1000 mL of DI water for a week. A lower swelling rate and a reduced swelling ratio are observed when the sample is soaked in DI water with a smaller volume. This is because the release of Na<sup>+</sup> and Cl<sup>−</sup> ions from the polymer composite results in a higher ion concentration in the external solution with a smaller volume and consequently a reduced osmotic pressure difference to drive the water influx.

In addition to the swelling performance, we characterize the mechanical properties of the polymer composite at different swelling states using tensile tests, and the stress–strain curves are plotted in Fig. S5(a) (ESI†). The sample before water immersion has a maximum tensile strain and critical stress before fracture of approximately 720% and 0.28 MPa, respectively. As immersion proceeds from 1 day to 3 days, the sample's maximum tensile strain and stress continually decrease to 130% and 0.012 MPa, 80% and 0.01 MPa, and 50% and 0.008 MPa, respectively. After drying, the sample's maximum tensile strain and stress recover to 370% and 0.15 MPa, respectively. The Young's modulus of the sample significantly decreases from 0.115 MPa to 0.018 MPa after one-day swelling but remains at the same level afterwards (Fig. S5(b), ESI†). Herein, we attribute the swelling-induced reduction in the mechanical strength of those polymer composites to the stretching of the polymer caused by the swelling, which can damage the polymer chain network. We present a summary of the swelling capability and Young's modulus of various swellable soft materials in comparison to our polymer composite in Fig. 1. Clearly, our polymer composite possesses a large swelling ratio and high stiffness simultaneously that has not been previously reported in the literature.

## 2.2. Osmosis-driven programmable shape transformation

The achievable large volumetric swelling ratio and relatively high stiffness of our polymer composite make it an ideal





material for shape-morphing functional structures and devices. We first combine the Ecoflex<sup>00-10</sup>/NaCl polymer composite and PDMS to form a bilayer structure. Because PDMS does not swell in water, curvature emerges in the initially straight bilayer beam as a result of the differential swelling in the active polymer composite and passive PDMS layers (Fig. 3(a)). As swelling continuously propagates from the outer surface of the polymer composite layer towards the inner part, curvature continuously increases until the polymer composite layer is fully swelled.

Extending from the simple bilayer structure, more complex shape-morphing structures are achieved by harnessing the strain mismatch between the swellable polymer composite

and non-swelling PDMS. As shown in Fig. 3(b–e), a star-shaped and a leaf-shaped shape-morphing structures are developed. For the star-shaped structure, the Ecoflex<sup>00-10</sup>/NaCl polymer composite strips are locally semi-embedded into the central axis of each horn of the pentagram made of PDMS. For the leaf-shaped one, the vein and lamina are composed of the Ecoflex<sup>00-10</sup>/NaCl polymer composite and PDMS, respectively. As the top surfaces of these polymer composite strips are exposed to the external environment, these active parts begin to absorb water and swell after the whole structure is immersed under water. With the increasing swelling in the polymer composite strips, the strain mismatch between the polymer composite strips and the PDMS matrix is gradually enhanced,

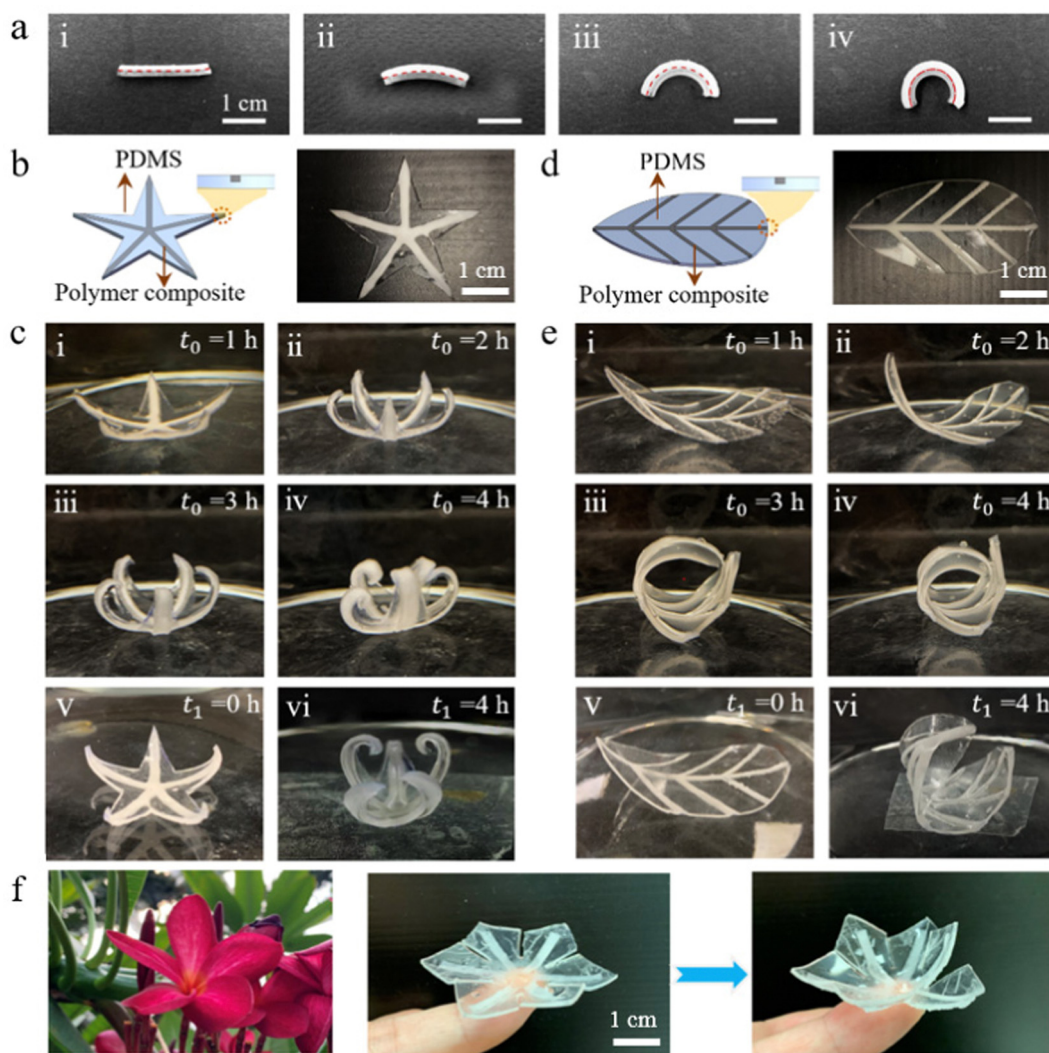


**Fig. 3** Swelling-induced shape morphing of a polymer composite-PDMS bilayer and PDMS structures with semi-embedded polymer composite strips. (a) Bending deformation of a polymer composite-PDMS bilayer structure after immersion in water. (b) An image of a star-shaped structure consisting of polymer composite strips semi-embedded in PDMS, along with its illustrative configuration. (c) Shape morphing of the sample in (b) at different stages (Panels i–iv: progressive shape-morphing process as immersion extends from one to four hours; Panels iv and v: morphed shape partially recovers with drying; Panels v and vi: re-morphing after putting the sample back in water). (d) A leaf-shaped structure consisting of polymer composite strips semi-embedded in PDMS, along with its illustrative configuration. (e) Shape morphing of the sample in (d) at different stages (Panels i–iv: progressive shape-morphing process as immersion extends from one to four hours; Panels iv and v: morphed shape partially recovers with drying; Panels v and vi: re-morphing after putting the sample back in water). (f) Shape morphing of a flower-shaped shape-morphing structure from a 2D flower pattern to a 3D blooming flower structure as a result of the swelling of the semi-embedded polymer composite strips.



leading to a progressive shape-morphing process, as shown from (i) to (iv) in Fig. 3(c) and (e). Once the swollen sample is dried, the morphed shape partially recovers (from (iv) to (v) in Fig. 3(c) and (e)). The incomplete restoration can be attributed to several factors. Firstly, some NaCl molecules reposition during the swelling stage and are trapped within the polymer after the structure is dried, thereby impeding polymer shrinkage. Additionally, the softening and plastic deformation of the polymer composite caused by an excessively high strain also prevent the complete shape recovery of the polymer composites (Fig. S6, ESI†). The heavily curved shape can be achieved again after putting the sample back in water (from (v) to (vi) in Fig. 3(c) and (e)).

To further investigate the repeatability of the shape change, we conduct a cyclic soaking-drying experiment for our polymer

composite. As displayed in Fig. S7 (ESI†), a conspicuous swelling with a volume swelling ratio of 1800% can still be observed after 6 times of immersion process although the swelling ratio drops by  $\sim 25\%$ . The drop of the swelling ratio is due to the slow release of  $\text{Na}^+$  and  $\text{Cl}^-$  ions from the polymer composite (Fig. S8, ESI†). The polymer composite exhibits excellent shape recovery with a small non-zero residual volume swelling ratio ( $< 100\%$ ) after each drying treatment. Notably, the rolling and twisting deformations in a rectangular PDMS strip can be achieved through meticulous geometric design, particularly by programming the angle formed between the active polymer composite stripes and the PDMS strip (Fig. S9, ESI†). A reversed flower opening process also can be vividly realized by programming the swellable polymer composite into the PDMS petals, as shown in Fig. 3(f). A 2D flower pattern gradually changes to a

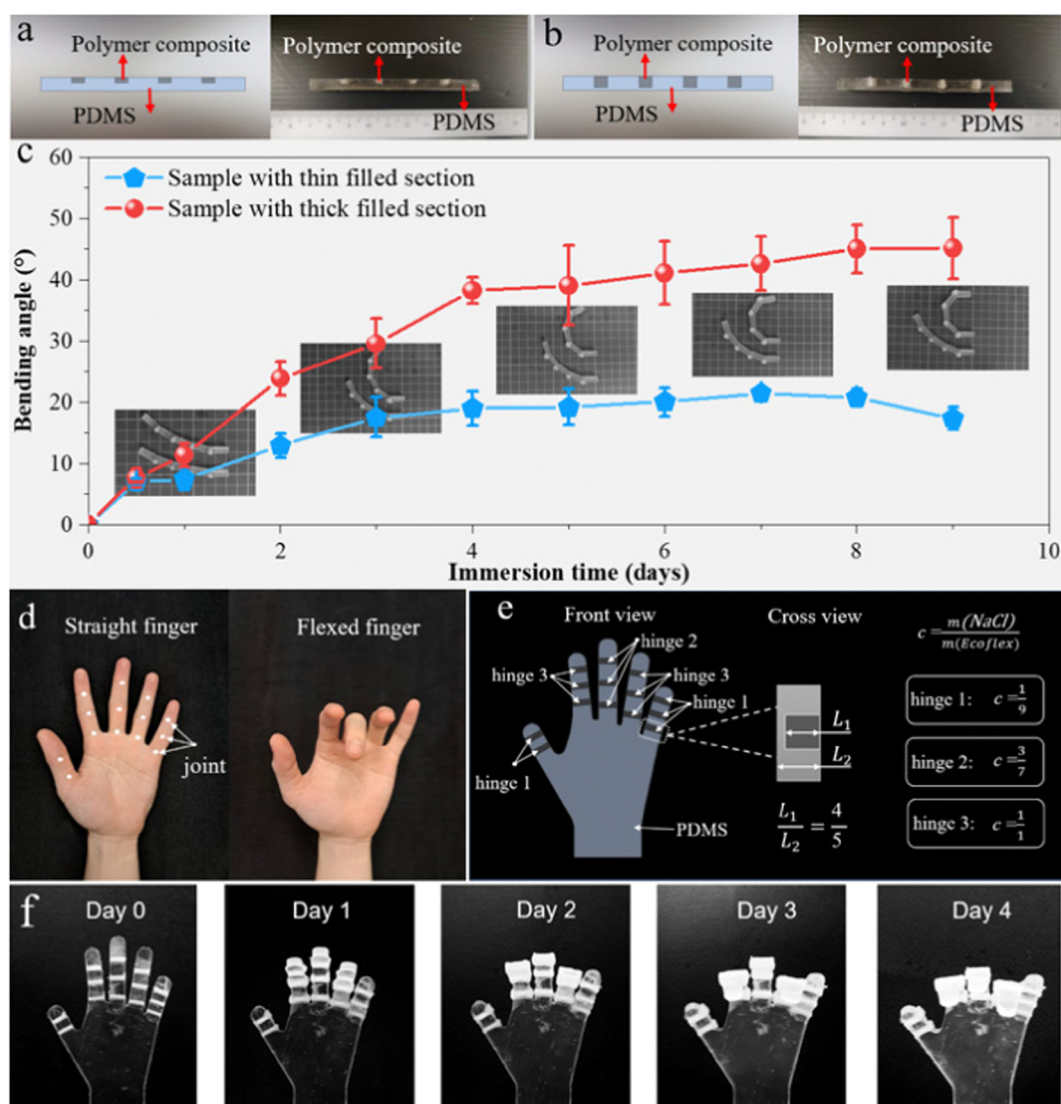


**Fig. 4** Swelling-induced sequential shape morphing of PDMS structures with semi-embedded Ecoflex<sup>00-10</sup>/NaCl polymer composite stripes. (a) and (b) Schematics and physical samples of 5 mm-thick PDMS strips with semi-embedded swellable polymer composite with a thickness of 2.5 mm and 4 mm, respectively. (c) Temporal evolution of the bending angle of the two samples in (a) and (b) during the immersion over 9 days. (d) Finger joint-driven adjustment of human fingers from straight to flexed. (e) Geometric design and material selection for the construction of a biomimetic human hand using swellable polymer composite as the joint hinges. (f) Progressive bending of the biomimetic hand during the immersion over 4 days.



3D blooming flower structure as a result of the swelling of semi-embedded polymer composite after immersed in water. Noted that here we only demonstrate several simple examples of shape-morphing structures. It can be expected that more convoluted shapes can be achieved by integrating rational design strategies, such as mechanics-informed inverse design and machine learning aided design.<sup>39–41</sup>

Sequential shape morphing refers to an encoded spatial and/or temporal shape evolution.<sup>42</sup> We first demonstrate a geometry-enabled sequential shape morphing by adopting our swellable polymer composite as active hinge structures. As shown in Fig. 4(a–b), swellable polymer composite strips of two different thicknesses (2.5 mm and 4 mm) are embedded into straight PDMS beams with a thickness of 5 mm. Fig. 4(c) records the evolution of the bending angles of the PDMS beams while the two structures are immersed in water for 9 days. During the initial immersion stage ( $t < 12$  h), these two samples possess a similar bending deformation, because the driving forces to bend these two bilayer structures are the same before the swelling of the thicker polymer composite strips reaches beyond a depth of 2.5 mm from the outer surface. As the immersion time further increases, the structure

with thicker strips features a larger driving force for bending, leading to a higher increasing rate in bending angle. The swelling of the thinner strips reaches saturation after 7 days before the bending angle starts to drop, however, the structure with thicker strips continues to bend more within 9 days. Furthermore, zigzag-shaped bending are achieved by placing the swellable strips alternatively on the two sides of the PDMS strip (Fig. S10, ESI†). The structure with thicker swellable strips exhibits a higher folding level.

Based on the concept of using swellable polymer composite as hinges to achieve sequential shape morphing, we develop a biomimetic hand by semi-embedding Ecoflex<sup>00–10</sup>/NaCl polymer composite into a hand-shaped PDMS structure to function as finger joints. As illustrated in Fig. 4(d), various finger postures can be achieved by controlling the bending angles of finger joints. To imitate these actions, we design a shape-morphing structure that resembles the shape of a human hand using PDMS, as shown in Fig. 4(e). Various polymer composite strips, which serve as finger hinges, are semi-embedded into the PDMS hand. All these hinges have the same geometry but different compositions. Based on the influence of NaCl

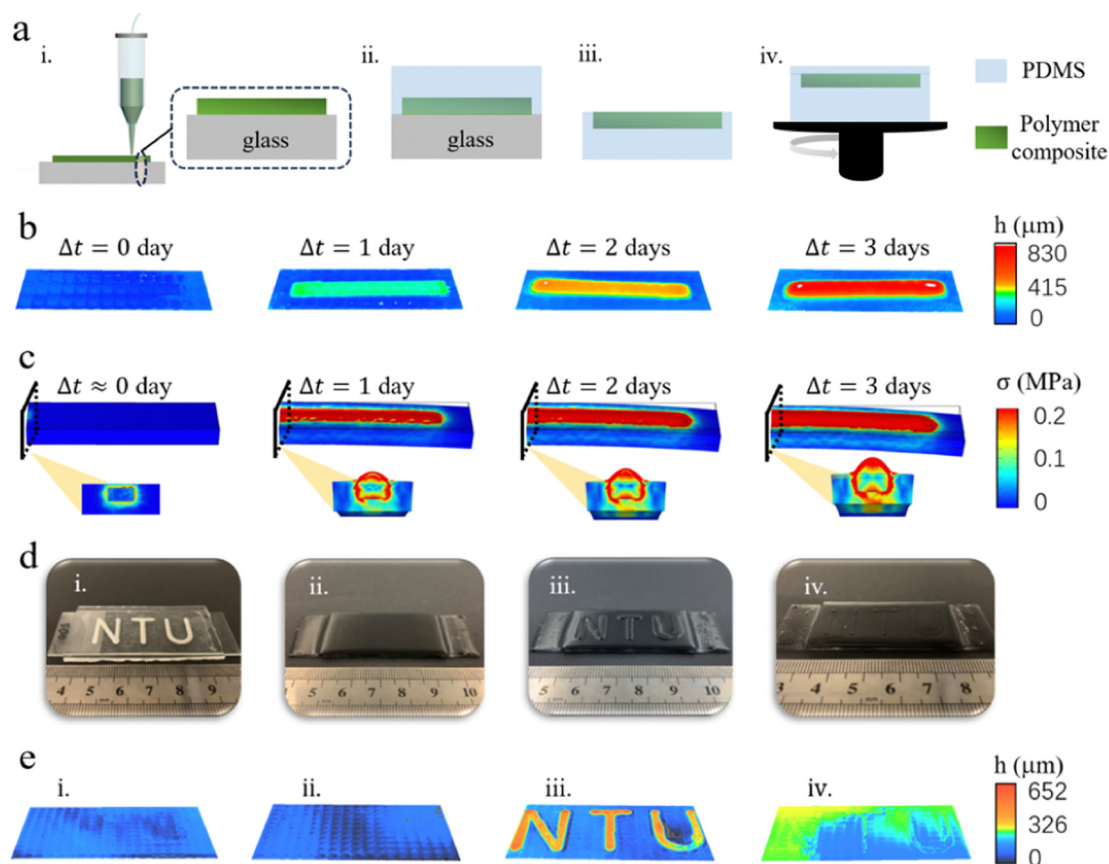


**Fig. 5** Fabrication and shape morphing of PDMS structures with fully embedded polymer composite for information encryption. (a) Schematic illustration of the fabrication process to fully embed 3D printed polymer composite patterns into PDMS. (b) Evolution of the 3D surface morphology of the PDMS sample with a fully embedded polymer composite strip after immersion in water. (c) COMSOL simulation presenting the von Mises stress distribution accompanied by shape change of the sample in (b). (d) Fabrication of Braille "NTU" with a visual and tactile regulation (Panel i: swellable "NTU" polymer composite strips wrapped by the pure PDMS to form Braille without a tactile difference; Panel ii: swellable "NTU" wrapped by the colored PDMS to form Braille without visual and tactile differences; Panel iii: visual and tactile "NTU" Braille triggered via immersion in water; Panel iv: partial recovery of triggered "NTU" Braille via drying). (e) 3D morphology changes corresponding to Panel (d).





concentration on the swelling of the polymer composite, we obtain a sequential bending deformation of the biomimetic hand in a programmable manner (Fig. 4(f)). As expected, the hinge with higher NaCl concentration causes finger bending to a larger angle, and *vice versa*.

### 2.3. Programmable braille with tactile regulation

Our polymer composite possesses exceptional capability of programmable swelling, making it highly suitable for applications in information encryption.<sup>43</sup> Herein, we manifest the design of a programmable braille that enables tactile regulation by fully embedding our swellable polymer composite into PDMS. As illustrated in Fig. 5(a), we utilize an extrusion-based 3D printer to write down the message using the polymer composite on a glass slide. For proof of concept, a simple strip pattern with dimensions of 20 mm (*L*) × 1 mm (*W*) × 0.5 mm (*H*) is created. After curing, liquid PDMS is poured onto the glass slide to encapsulate the polymer composite pattern. After curing, the PDMS, along with the encapsulated polymer composite, is carefully peeled off from the glass slide. We then spin-coat an additional layer of liquid PDMS onto the exposed surface of polymer composite to cover and hide the message. Spin-coating is conducted under 500 rpm for 60 s. The hidden message can be revealed by immersing the sample in water. As PDMS is water-permeable,<sup>44–46</sup> water molecules can permeate the PDMS film and reach the embedded Ecoflex<sup>00–10</sup>/NaCl polymer composite strip. As the strip swells, it induces an out-of-plane deformation of the PDMS film, thereby exposing the patterns beneath the PDMS film. These patterns can be readily discerned through tactile reading, akin to reading braille.

We capture the 3D surface morphologies of the sample at different stages using a laser scanning microscope (Fig. 5(b)). Before immersion in water, the thin PDMS film depicts a flat and smooth surface. However, upon soaking in water under 60 °C for 1–3 days, we observe localized deformation above the polymer composite strips, resulting in a surface elevation of 200 μm, 450 μm and 730 μm, respectively. The surface elevation level gradually decreases when the sample is allowed to dehydrate in the ambient air and recovers after re-soaking the dehydrated sample in water (Fig. S11, ESI†), confirming its reusability. To further analyze the morphing process, COMSOL simulation is performed, which clearly illustrates the progressive out-of-plane deformation of the thin PDMS layer directly above the swelling strips (Fig. 5(c)). It is worth noting that stress concentration occurs at the interface between the polymer composite and the surrounding PDMS matrix, and this concentration increases with the swelling level.

The extent of the out-of-plane bending deformation of the PDMS surface directly above the swellable strips can be adjusted by varying the thickness of the PDMS layer using different spin-coating speeds (see Fig. S12, ESI†). As expected, the heights of the samples show a positive correlation with the immersion time (Fig. S13 and S14, ESI†). The increase in sample height is more pronounced for the sample fabricated at a higher spin-coating speed, as a thinner PDMS layer exerts less mechanical restraint on the swelling of the polymer composite strips. Moreover, a thinner PDMS layer facilitates

easier transport of water molecules, resulting in a higher swelling rate. However, it is important to note that, during immersion, Na<sup>+</sup> and Cl<sup>−</sup> ions can be transported through the thin PDMS layer and subsequently released, leading to a slight reduction in the sample height compared to its original dimension after the drying process.

With 3D printing, complex information can be easily customized and encrypted into our programmable braille design. To demonstrate this capability, we fully embed our polymer composite with the “NTU” pattern into PDMS, following the same fabrication protocol. Fig. 5(d)(i) shows the clearly visible “NTU” pattern beneath the smooth and flat surface of PDMS (Fig. 5(e)(i) and Fig. S15(a), ESI†). To address the visual difference, we introduce approximately 5 wt% of iron nanoparticles into the liquid PDMS, resulting in a sample that exhibits no discernible visual and tactile difference (Fig. 5(d)(ii) and (e)(ii) and Fig. S15(b), ESI†). Subsequently, we immerse the sample in DI water under 60 °C. After soaking for 1–2 days, the word of “NTU” becomes both visually (Fig. 5(d)(iii)) and tactually perceptible through surface topology scanning (Fig. 5(e)(iii) and Fig. S15(c), ESI†). Herein, we emphasize that the emerged “NTU” can be partially erased. As shown in Fig. 5(d)(iv), (e)(iv) and Fig. S15(d) (ESI†), both visual and tactile differences are reduced significantly by drying the sample. Therefore, this shape-morphing phenomenon holds promise for employing programmable braille as a means of information encryption with visual and tactile regulation.

## 3. Conclusion

In this work, inspired by the osmosis-driven shape changes observed in living organisms, we designed a polymer composite system composed of NaCl powders and Ecoflex<sup>00–10</sup>, which exhibited both large swelling and high stiffness. We systematically investigated the effects of key factors, such as immersion temperature, sample thickness, and concentration of doped NaCl powders, on the swelling behavior. By leveraging the excellent swelling performance of our polymer composite and employing rational structural design, we demonstrated a facile strategy for fabricating shape-morphing structures. By exploiting the strain mismatch between different polymers and employing a semi-embedded structural layout, we have achieved tunable sequential deformation in polymer composite strips embedded in PDMS. The resulting shape change allowed us to resemble the human finger bending with different angles, showcasing its potential for applications in soft robotics. Furthermore, with swellable polymer composite fully encapsulated within the PDMS, we demonstrated the application of our polymer composite for a programmable braille. The demonstrated programmable braille holds great promise for information encryption.

## 4. Experimental section

### Fabrication of swellable polymer composite

The swellable polymer composite was created by mixing Ecoflex<sup>00–10</sup> silicone (Smooth on, Inc.) with fine sodium chloride (NaCl)





powders (ACS reagent, Sigma-Aldrich) in a weight ratio of 1:1, unless otherwise stated. The Ecoflex<sup>00-10</sup> was prepared by mixing Part A and B in a weight ratio of 1:1. The NaCl powders were manually grounded and sieved through a 50  $\mu\text{m}$ -pore sieve to achieve the desired fine particles before mixed with the Ecoflex<sup>00-10</sup>.

### Fabrication of shape-morphing structures

The bilayer polymer composite comprised of two distinct layers made of the swellable polymer composite and non-swellable polydimethylsiloxane (PDMS) (Sylgard 184, Dow Corning), respectively. PDMS was prepared by mixing the base and cure agents at a weight ratio of 10:1. To form the first PDMS layer, we filled liquid PDMS into a hollow mold with dimensions of 20 mm ( $L$ )  $\times$  5 mm ( $W$ )  $\times$  1 mm ( $H$ ), and let it cure at room temperature for one day. To fabricate the second layer, an identical mold was stacked closely onto the first mold to seal off any leakages and filled with Ecoflex<sup>00-10</sup>/NaCl polymer composite. A glass coverslip was utilized to level and seal the polymer composite until it fully cured. To fabricate samples with semi-embedded polymer composite structures, we modified the hollow mold by mounting one end with a square wave patterned acrylic sheet. The specific dimensions of the square wave pattern were described in the Results and Discussion section. Liquid PDMS was then poured into this modified mold and allowed to cure at room temperature for one day. Upon peeling off the modified mold, a PDMS structure with specific square wave voids was obtained. Finally, the voids were filled with the Ecoflex<sup>00-10</sup>/NaCl polymer composite, and a cover glass was used to level and seal the polymer composite until it fully cured. To fabricate the PDMS structure with fully embedded polymer composite, we started with 3D printing the polymer composite onto a glass slide placed inside a Petri dish and allowing it to fully cure. Using the 3D printer, we fabricated various patterns with controlled dimensions, including a strip measuring 20 mm ( $L$ )  $\times$  1 mm ( $W$ )  $\times$  0.5 mm ( $H$ ) and letter patterns spelling “NTU” with dimensions of 1 mm ( $W$ )  $\times$  0.5 mm ( $H$ ). Subsequently, we poured liquid PDMS into the Petri dish to encapsulate the printed polymer composite patterns. The thickness of this PDMS layer was fixed at 2.5 mm. After curing, the PDMS layer with the encapsulated polymer composite was carefully peeled off from the glass slide. An additional layer of liquid PDMS was then spin-coated onto the surface of polymer composite. The thickness of this layer was varied by employing different spin-coating speeds. All the molds were prepared by cutting acrylic sheets using a laser cutter. For extrusion-based 3D printing, the desired 3D model was created using CAD software (SolidWorks). The 3D printer (BIO XTM, 3D BioPRINTER, CELLINK) with a tapered nozzle (400  $\mu\text{m}$  in diameter, Nordson) was used to fabricate the desired structure. The following printing parameters were adopted, including extrusion pressure of 1.5 bar, printing speed of 10 mm s<sup>-1</sup>, pre-flow of 0.2 sec, and post-flow of 0 sec, to ensure uniform deposition and high printing quality.

### Characterization of the swelling behavior of the polymer composite

To quantitatively assess the swelling process, a Vernier caliper and a scale were used to measure the dimension and weight of

the sample, respectively, before soaking and after each 24-hours period of immersion in DI water under various temperatures. Under the default condition, 1 L of DI water was used and refreshed after each immersion period. The water absorption (WA) and volume swelling (VS) ratios were calculated based on  $WA (\%) = [(m_1 - m_0)/m_0] \times 100\%$  and  $VS (\%) = [(V_1 - V_0)/V_0] \times 100\%$ , where  $m_0$  and  $m_1$  are the mass of the polymer composite before and after immersion, respectively, and  $V_0$  and  $V_1$  are the volume of the polymer composite before and after immersion, respectively.<sup>47</sup> The global shape transformations were recorded using a camera. The local morphologies of the samples were observed using a field-emission scanning electron microscope (FE-SEM, HITACHI, SU-70) with operating voltage of 5 kV and 3D Laser Scanning Microscopy (VK-X1000, KEYENCE).

### Mechanical property characterization

Mechanical properties of the fabricated samples were characterized using a tensile tester (Instron, 3366) at room temperature. The specimens were mounted to the instrument with gauge length of 10 mm, wide of 10 mm, and thickness of 1 mm. Tensile testing was conducted with a stretching speed of 15 mm s<sup>-1</sup>.

### COMSOL simulation

Computational analyses were conducted using the commercial numerical analysis software (COMSOL Multiphysics) to simulate the swelling-induced deformation of the sharp-morphing structures. In the simulation, we simulated the process of water molecule diffusing into the shape-morphing structures. The water diffusion process follows the diffusion equation:

$$\frac{\partial c}{\partial t} + \nabla \cdot (-D\nabla c) = 0 \quad (1)$$

where  $c$  is real-time concentration of water molecule, and  $D$  is the diffusion coefficient of water molecule. In the meantime, the hygroscopic swelling is governed by the following equation,

$$\varepsilon = \beta M(c - c_0) \quad (2)$$

where  $\varepsilon$  is swelling-induced mechanical strain,  $\beta$  the coefficient of hygroscopic swelling (*i.e.*, the ratio of the volume swelling and the water absorption),  $M$  the molar mass of water, and  $c_0$  the original concentration of water molecule. Here we set the pure water concentration outside the shape-morphing structure as 55.5 mol L<sup>-1</sup> and the initial water concentration inside Ecoflex<sup>00-10</sup>/NaCl composite and PDMS as 0, and set water molar mass as 0.018 kg mol<sup>-1</sup>. From our experiment, the volume of PDMS did not change in water, which means

**Table 1** Summary of the material properties adopted in simulations

Property	PDMS	Ecoflex <sup>00-10</sup> /NaCl composite
Coefficient of hygroscopic swelling (m <sup>3</sup> kg <sup>-1</sup> )	0	0.0015 <sup>23</sup>
Diffusion coefficient (m <sup>2</sup> s <sup>-1</sup> )	4 $\times$ 10 <sup>-12</sup>	4 $\times$ 10 <sup>-17</sup>
Young's modulus (kPa)	1603	115
Poisson's ratio	0.49	0.315



$\beta_{\text{PDMS}} = 0$ . The coefficient of hygroscopic swelling of Ecoflex<sup>00-10</sup>/NaCl was calculated based on the reported work ( $\beta_{\text{Ecoflex/NaCl}} = 0.0015 \text{ m}^3 \text{ kg}^{-1}$ ).<sup>23</sup> All the geometric dimensions of the numerical models were adopted based on the samples used in experiments. The material properties of PDMS and Ecoflex<sup>00-10</sup>/NaCl composite were summarized in Table 1. In particular, the diffusion coefficients were fitted by matching the running time of simulation with the experimental result.

## Conflicts of interest

There are no conflicts of interest to declare.

## Acknowledgements

M. L. acknowledges the Presidential Postdoctoral Fellowship from Nanyang Technological University, Singapore, and the Start-up funding from the University of Birmingham. C.H. acknowledges financial support from Ministry of Education (MOE), Singapore, under its Academic Research Fund Tier 1 (RG74/23) and Academic Research Fund Tier 2 (MOET2E P50121-0004).

## References

- H. Kim, S.-k Ahn, D. M. Mackie, J. Kwon, S. H. Kim, C. Choi, Y. H. Moon, H. B. Lee and S. H. Ko, *Mater. Today*, 2020, **41**, 243–269.
- P. Lv, X. Yang, H. K. Bisoyi, H. Zeng, X. Zhang, Y. Chen, P. Xue, S. Shi, A. Priimagi, L. Wang, W. Feng and Q. Li, *Mater. Horiz.*, 2021, **8**, 2475–2484.
- S. Armon, E. Efrati, R. Kupferman and E. Sharon, *Science*, 2011, **333**, 1726–1730.
- X. Le, W. Lu, J. Zhang and T. Chen, *Adv. Sci.*, 2019, **6**, 1801584.
- D. Jiao, Q. L. Zhu, C. Y. Li, Q. Zheng and Z. L. Wu, *Acc. Chem. Res.*, 2022, **55**, 1533–1545.
- A. Kumar, R. Rajamanickam, J. Hazra, N. R. Mahapatra and P. Ghosh, *ACS Appl. Mater. Interfaces*, 2022, **14**, 56321–56330.
- B. Rivkin, C. Becker, F. Akbar, R. Ravishankar, D. D. Karnaushenko, R. Naumann, A. Mirhajivarzaneh, M. Medina-Sánchez, D. Karnaushenko and O. G. Schmidt, *Adv. Intell. Syst.*, 2021, **3**, 2000238.
- C. Wang, K. Sim, J. Chen, H. Kim, Z. Rao, Y. Li, W. Chen, J. Song, R. Verduzco and C. Yu, *Adv. Mater.*, 2018, **30**, 1706695.
- Z. Ding, H. Zreiqat and M. Mirkhalaf, *Mater. Horiz.*, 2022, **9**, 2762–2772.
- R. Goyal and S. Mitra, *Front. Mater.*, 2022, **9**, 837923.
- A. J. Hughes, H. Miyazaki, M. C. Coyle, J. Zhang, M. T. Laurie, D. Chu, Z. Vavrušová, R. A. Schneider, O. D. Klein and Z. J. Gartner, *Dev. Cell*, 2018, **44**, 165–178.
- X. Liu, M. Gao, J. Chen, S. Guo, W. Zhu, L. Bai, W. Zhai, H. Du, H. Wu and C. Yan, *Adv. Funct. Mater.*, 2022, **32**, 2203323.
- S. Xu, Z. Yan, K.-I. Jang, W. Huang, H. Fu, J. Kim, Z. Wei, M. Flavin, J. McCracken and R. Wang, *Science*, 2015, **347**, 154–159.
- O. Erol, A. Pantula, W. Liu and D. H. Gracias, *Adv. Mater. Technol.*, 2019, **4**, 1900043.
- T. Billiet, M. Vandenhaute, J. Schelfhout, S. Van Vlierberghe and P. Dubruel, *Biomaterials*, 2012, **33**, 6020–6041.
- S.-J. Liang, R. M. Fitch and J. Ugelstad, *J. Colloid Interface Sci.*, 1984, **97**, 336–347.
- A. M. Abdullah, P. V. Braun and K. J. Hsia, *Appl. Phys. Lett.*, 2017, **111**, 104101.
- J. N. Lee, C. Park and G. M. Whitesides, *Anal. Chem.*, 2003, **75**, 6544–6554.
- M. Cesaria, V. Arima, M. G. Manera and R. Rella, *Polymer*, 2018, **139**, 145–154.
- N. Dehbari and Y. Tang, *J. Appl. Polym. Sci.*, 2015, 132.
- L. M. Polgar, F. Fallani, J. Cuijpers, P. Raffa, A. A. Broekhuis, M. van Duin and F. Picchioni, *Rev. Chem. Eng.*, 2018, **35**, 45–72.
- Y. Yang, S. Duan and H. Zhao, *Adv. Mater. Interfaces*, 2021, **8**, 2100137.
- Y. Yang, S. Duan, W. Xiao and H. Zhao, *Sens. Actuators, A*, 2022, **343**, 113653.
- L. Zhu, J. Qiu and E. Sakai, *RSC Adv.*, 2017, **7**, 43755–43763.
- K.-i Hoshino, T. Nakajima, T. Matsuda, T. Sakai and J. P. Gong, *Soft Matter*, 2018, **14**, 9693–9701.
- R. Subramani, A. Izquierdo-Alvarez, P. Bhattacharya, M. Meerts, P. Moldenaers, H. Ramon and H. Van Oosterwyck, *Front. Mater.*, 2020, **7**, 212.
- L. Wang, F. Liu, J. Qian, Z. Wu and R. Xiao, *Soft Matter*, 2021, **17**, 10421–10427.
- A. Kataruka and S. B. Hutchens, *Matter*, 2021, **4**, 3991–4005.
- D. Fraser, T. Nguyen, A. Kotelsky, W. Lee, M. Buckley, D. S. Benoit and Engineering, *ACS Biomater. Sci.*, 2022, **8**, 3568–3575.
- J. Ren, Y. Liu, Z. Wang, S. Chen, Y. Ma, H. Wei and S. Lü, *Adv. Funct. Mater.*, 2022, **32**, 2107404.
- J. Zhou, Y. Huang, S. Qian, P. Zeng, S. Long and X. Li, *Mater. Lett.*, 2022, **324**, 132582.
- S. Bian, L. Hao, X. Qiu, J. Wu, H. Chang, G. M. Kuang, S. Zhang, X. Hu, Y. Dai and Z. Zhou, *Adv. Funct. Mater.*, 2022, **32**, 2207741.
- Q. Bian, L. Fu and H. Li, *Nat. Commun.*, 2022, **13**, 1–8.
- X. P. Hao, C. W. Zhang, W. Hong, M. Meng, L. X. Hou, M. Du, Q. Zheng and Z. L. Wu, *Mater. Horiz.*, 2023, **10**, 432–442.
- X. Yang, X. Zhou, H. Zhao, W. Huang, Y. Wang, K. J. Hsia and M. Liu, *Soft Sci.*, 2023, **3**, 38.
- R. K. Manna, O. E. Shklyayev, H. A. Stone and A. C. Balazs, *Mater. Horiz.*, 2020, **7**, 2314–2327.
- M. J. Lopez and C. A. Hall, *StatPearls [Internet]*, 2022, PMID 32491541.
- C. Yang, X. Xing, Z. Li and S. Zhang, *Polymers*, 2020, **12**, 138.
- M. Liu, L. Domino and D. Vella, *Soft Matter*, 2020, **16**, 7739–7750.
- H. Kansara, M. Liu, Y. He and W. Tan, *J. Mech. Phys. Solids*, 2023, **180**, 105382.
- T. Jin, X. Cheng, S. Xu, Y. Lai and Y. Zhang, *J. Mech. Phys. Solids*, 2023, **179**, 105398.



- 42 R. Guseinov, C. McMahan, J. Pérez, C. Daraio and B. Bickel, *Nat. Commun.*, 2020, **11**, 237.
- 43 Z. Meng, H. Yan, M. Liu, W. Qin, G. M. Genin and C. Q. Chen, *Adv. Sci.*, 2023, **10**, 2301581.
- 44 T. Merkel, V. Bondar, K. Nagai, B. Freeman and I. Pinnau, *J. Polym. Sci., Part B: Polym. Phys.*, 2000, **38**, 415–434.
- 45 A. Borde, M. Larsson, Y. Odelberg, J. Hagman, P. Löwenhielm and A. Larsson, *Acta Biomater.*, 2012, **8**, 579–588.
- 46 R. Riesco, L. Boyer, S. Blosse, P. M. Lefebvre, P. Assemat, T. Leichle, A. Accardo and L. Malaquin, *ACS Appl. Mater. Interfaces*, 2019, **11**, 28631–28640.
- 47 Y. Yang and H. Zhao, *Appl. Surf. Sci.*, 2022, **577**, 151895.

